Environmental Science and Pollution Research (2021) 28:5966–5977
https://doi.org/10.1007/s11356-020-10970-2

RESEARCH ARTICLE

Preparation of multi-walled carbon nanotubes based magnetic multi-template molecularly imprinted polymer for the adsorption of phthalate esters in water samples

Dongli Deng[1,2] · Yingnan He[1] · Mingyuan Li[1] · Ludan Huang[1] · Jinzhong Zhang[1]

Received: 12 May 2020 / Accepted: 21 September 2020 / Published online: 26 September 2020

Abstract

Taking the advantages of surface imprinting, multi-template imprinting and magnetic separation, a novel magnetic multi-template molecularly imprinted polymer (mag-MMIP@MWCNTs) was prepared by using MWCNTs as support material, Fe_3O_4 as magnetic core, and dimethyl phthalate (DMP), diethyl phthalate (DEP), and dibutyl phthalate (DBP) as template molecules. This composite was characterized by scanning electron microscopy (SEM), Fourier-transform infrared spectroscopy (FTIR), vibrating sample magnetometer (VSM), and the Brunauer-Emmett-Teller (BET) analysis, and was used for the simultaneous adsorption of DMP, DEP, and DBP in aqueous solution. The effects of solution pH, contact time, PAEs initial concentration, temperature, adsorption selectivity, and reusability were investigated and discussed in detail. The results demonstrated that mag-MMIP@MWCNTs exhibited fast kinetics, good magnetic separation, and excellent selectivity for the adsorption of three phthalate esters (PAEs). The adsorption kinetics followed pseudo second-order kinetic model and the adsorption thermodynamics followed Langmuir isothermal model very well, and the maximum adsorption capacities (Q_{max}) of DMP, DEP, and DBP were obtained as 0.95, 1.38, and 7.09 mg g^{-1}, respectively. The Scatchard analysis revealed that the template-polymer system had a two-site binding behavior. The adsorption thermodynamic studies indicated that the adsorption processes were exothermic and spontaneous, and dominated by physical adsorption relying on hydrogen bond, hydrophobic interaction, and van der Waals force. Mag-MMIP@MWCNTs also showed good reproducibility and reusability for simultaneous adsorption of the three PAEs. The potential application of mag-MMIP@MWCNTs was proved by the removal of DMP, DEP, and DBP spiked in environmental water samples.

Keywords Magnetic molecularly imprinted polymer · Multi-template · Phthalate esters · Simultaneous adsorption · Environmental water samples

Introduction

Phthalate esters (PAEs) are synthetic organic compounds and intensively used as important additives in plastic industry (Gani and Kazmi 2016; Oca et al. 2016). Since PAEs are not chemically bound with the polymeric matrix, they can be released from plastic materials into the environment. In China, some PAEs were ubiquitous in water environment, e.g., dibutyl phthalate (DBP) and di-(2-ethylhexyl) phthalate (DEHP) were the most frequently detected, and followed by dimethyl phthalate (DMP) and diethyl phthalate (DEP) (Ding et al. 2019; Liu et al. 2014; Net et al. 2015). In the USA, it was reported that the highest concentrations of DEP and DBP in groundwater were 147 and 50 μg·L^{-1}, respectively (Gani et al. 2017). As a kind of synthetic environmental hormones, PAEs in water environment can produce reproductive toxicity to

Responsible Editor: Tito Roberto Cadaval Jr

Electronic supplementary material The online version of this article (https://doi.org/10.1007/s11356-020-10970-2) contains supplementary material, which is available to authorized users.

✉ Jinzhong Zhang
jzhzhang@swu.edu.cn

[1] College of Resources and Environment, Southwest University, Chongqing Key Laboratory of Agricultural Resources and Environment, Chongqing 400715, People's Republic of China

[2] Chemical Pollution Control and Applied Technology Extension Center of Chongqing Higher Vocational Colleges, Chongqing Industry, Polytechnic College, Chongqing 401120, People's Republic of China

aquatic organisms, and may pose a potential threat to human health (Chen and Sung 2005; Net et al. 2015; Wang et al. 2015). Therefore, PAEs have been regarded as a kind of priority pollutants for risk assessment in many countries and regions, and it is of great significance to develop a simple and effective method to remove PAEs in water environment (Yang et al. 2015).

In order to remove PAEs in the polluted water, some methods including biodegradation, adsorption, and advanced oxidation are available (Abdel daiem et al. 2012). Among these methods, adsorption is considered a simple and efficient method because of its easy operation, cost-effectiveness, and high regeneration ability, which has been widely used in industry to remove pollutants (Awual et al. 2019b; Julinová and Slavík 2012). Until now, activated carbon (Fang and Huang 2010; Jedynak et al. 2017), biochars (Yao et al. 2019; Zhang et al. 2016), carbon nanotubes (Abdul et al. 2015; Wang et al. 2010), polymeric resin (Xu et al. 2011), chitosan (Chen et al. 2007; Shaida et al. 2018), clay minerals (Wu et al. 2015), and some new composite materials (e.g., zeolitic imidazolate and metal-organic frameworks, alkylbenzene-functionalized polypropylene nonwoven, and biochar graphene nanosheet composites) (Abdul et al. 2017; Khan et al. 2015; Zhang et al. 2018) have been used as adsorbents to remove PAEs in water. Under the given conditions, the adsorption performances of these materials have been confirmed, but the adsorption processes need to take several hours or even longer time to attain equilibrium, and filtration or centrifugation procedure is required to separate the adsorbents from aqueous phase, which is very time-consuming and cumbersome. Moreover, PAEs are commonly present at very low concentration and always coexist with a variety of toxic and non-biodegradable pollutants in water environment, which is a great challenge for selective adsorption of PAEs. So further development of new materials is still needed to break through some technical bottlenecks, such as the lack of molecular selectivity, low kinetics to target molecule, and cumbersome filtration or centrifugation procedure.

As a kind of synthetic macroporous materials, molecularly imprinted polymers (MIPs) can create structurally complementary recognition sites to match template compounds with similar structure (Chen et al. 2016). Due to their features of high selectivity, chemical stability, and wide adaptability, MIPs have been used in the studies on wastewater treatment in recent years, and are considered to be one kind of the most promising adsorbents for pollutant removal in aqueous phase (Huang et al. 2015). Owning to superparamagnetic effect, magnetic nanoparticles (MNPs) can be easily used for the rapid separation of solid and liquid phases. Using MNPs as "core", surface MIPs bound target molecules can be easily collected and separated by an external magnetic field without filtration or centrifugation, which simplifies further treatment process and avoids secondary pollution caused by residual adsorbent (Kumar et al. 2018). Moreover, the surface imprinting composite can not only selectively recognize the template molecules in complex matrix, but also effectively avoids the deficiencies of traditional imprinting technology, such as template leakage, large size, irregular morphology, and low mass transfer efficiency (Li et al. 2018). Therefore, combining MNPs with MIPs, magnetic MIPs could be the promising multifunctional candidate for selective separation and effective removal of target pollutants, which have been attracted increasing attention (Guo et al. 2019; Pan et al. 2011; Zuo et al. 2019).

At present, most MIPs were prepared using single template in many researches, which restricts the recognition for a family of compounds. Based on the cross selectivity, the recognition of multiple substances can be simultaneously achieved by constructing multiple-matching imprinted recognition sites (Lu et al. 2017), and thus a multi-template imprinting strategy can be developed to improve the utilization efficiency of MIPs using two or more structural analogues as templates. Some studies have been focused on the application of multi-template MIPs, but they are mainly concentrated in the fields of solid-phase extraction and microsphere extraction (Madikizela and Chimuka 2016; Ostovan et al. 2018), and little attention has been paid to synthesize magnetic MIPs combining multi-template imprinting and magnetic separation technologies. As a result, there is a broad space for the development of magnetic multi-template MIPs as the adsorbent for pollutant removal in aqueous systems.

In this work, combining the merits of magnetic separation, surface imprinting and multiple-template imprinting, novel magnetic multi-template molecularly imprinted polymer (mag-MMIP@MWCNTs) based on multi-walled carbon nanotubes (MWCNTs), were prepared by using three frequently detected PAEs (DMP, DEP, and DBP) as template molecules, Fe_3O_4 as magnetic core, and MWCNTs as support material due to their nanoscale dimension, large specific surface area, and high dispersion and stability (Gao et al. 2012). The prepared material was characterized by SEM, FTIR, VSM, and BET analysis and was used to simultaneously adsorb the three PAEs in aqueous solution. The adsorption conditions were optimized, and the adsorption properties and mechanisms were illustrated by adsorption kinetics, isotherm, selectivity, and adsorbent reuse. The potential application of the material was testified to remove the three PAEs spiked in environmental water samples.

Materials and methods

Reagents and materials

Dimethyl phthalate (DMP), diethyl phthalate (DEP), dibutyl phthalate (DBP), di-(2-ethylhexylPhthalate (DEHP), phthalic

acid (H_2PA), methacrylic acid (MAA), ethylene dimethacrylate (EDMA), 2, 2-azobis(2-methylpropionitrile) (AIBN), 3-(trimethoxysilyl) propyl methacrylate (KH-570), and tetraethoxysilane (TEOS) were purchased from Shanghai Adamas Reagent Co., Ltd., China. Acetonitrile with HPLC grade was purchased from Fisher Scientific Inc., USA. Other reagents used in this study were provided by Chengdu Kelong Chemical Co., Ltd., China. Multi-walled carbon nanotubes (MWCNTs, 60–100 nm in diameter) were obtained from Shenzhen Nanotech Port Co., Ltd., China. All chemical reagents were of analytical grade and used without further purification. Ultra-pure water was used throughout the experiment.

Preparation of magnetic multi-template molecularly imprinted polymer

The preparation of mag-MMIP@MWCNTs via a multi-step procedure is shown in Fig. 1 and carried out as below.

Preparation of MWCNTs@Fe_3O_4@SiO_2-C=C composite: magnetic multi-walled carbon nanotubes (MWCNTs@Fe_3O_4) were first prepared according to the method of Rao et al. (Rao et al. 2014), and then coated on SiO_2 by the Stöber process (Luo et al. 2010). MWCNTs@Fe_3O_4 (0.50 g) was dispersed into 49.5 mL of anhydrous ethanol, and 6.3 mL of ultrapure water and 2.2 mL of TEOS were added in ice water bath with constant stirring for 10 min, and then 2.0 mL of 25% $NH_3{\cdot}H_2O$ (v/v) was added dropwise to adjust pH to alkaline. After stirring at room temperature for 12 h, the resultant product (MWCNTs@Fe_3O_4@SiO_2) was washed with anhydrous ethanol for 6 times, and dried in vacuum at 60 °C for 12 h. Afterwards, 0.5 g of MWCNTs@Fe_3O_4@SiO_2 was dispersed into 30 mL of 50% ethanol, and pH was adjusted to 4 with acetic acid, and then 1.5 mL of KH-570 was added and stirred at 50 °C for 24 h. The product was separated by an external magnetic field, washed with ethanol for several times, dried and stored under vacuum for further use, which was noted as MWCNTs@Fe_3O_4@SiO_2-C=C.

Preparation of magnetic multi-template molecularly imprinted polymer: 0.2 mmol of multi-template (n_{DMP}:n_{DEP}:n_{DBP} = 6:3:2), 0.8 mmol of MAA functional monomer and 50 mL of acetonitrile were mixed with ultrasound in a three-port bottle for 10 min, and then placed in the dark for 3 h allowing self-assembly of the three PAEs and MAA. Next, 100 mg of MWCNTs@Fe_3O_4@SiO_2-C=C, 4 mmol of EDMA cross-linker and 20 mg of AIBN initiator were mixed thoroughly, and degassed with ultrasound at 20 °C for 1 h to form a homogeneous dispersion. Under the protection of N_2 atmosphere, the mixture was polymerized in 60 °C water bath with constant stirring for 24 h, and the obtained product (mag-MMIP@MWCNTs) was washed several times with the mixed solution of methanol and acetic acid (9:1, v/v) to remove the multi-template. When the three templates in the elution solvent were not detected by HPLC, the product was washed with ethanol to neutral and dried under vacuum at 60 °C.

For contrast, the non-imprinted polymer (mag-NIP@MWCNTs) was synthesized using the above procedures without PAEs multi-template.

Instruments and analyses

The morphology of the prepared materials at different stages was investigated by the TESCAN MIRA3 scanning electron microscopy (SEM, Tescan, Czech) at an accelerating voltage of 5 kV, and the group characteristics were recorded by the Nicolet 6700 Fourier-transform infrared spectrometer (FTIR, Thermo Scientific, USA) in the wave number range of 4000–650 cm^{-1}. The magnetic property was analyzed by VSM 7037 vibrating sample magnetometer (VSM, Lake Shore, USA) at room temperature. The surface area and porosity were analyzed through N_2 adsorption-desorption experiment by the 2460 Brunauer-Emmett-Teller analyzer (BET, Micromeritics, USA).

DMP, DEP, and DBP were determined by an LC-20A high performance liquid chromatograph (HPLC, Shimadazu, Japan). Chromatographic separation was achieved in an Inertsil ODS-SP column (250 mm × 4.6 mm, 5 μm,

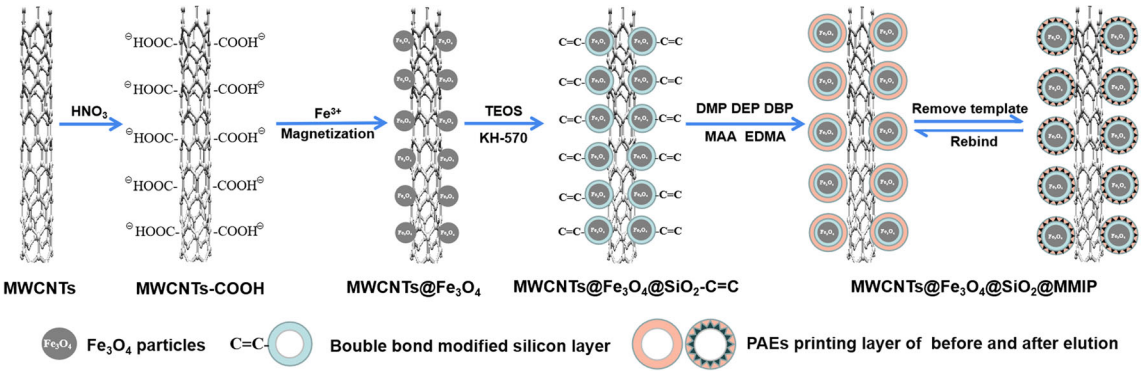

Fig. 1 Schematic diagram of the preparation of mag-MMIP@MWCNTs

Shimadazu GL-science, Japan) using acetonitrile and water as mobile phases at a flow rate of 1.0 mL min^{-1}. The gradient elution program started from 70% acetonitrile and held for 6 min, and then increased to 100% acetonitrile in 2 min and held for 8 min, finally returned to 70% acetonitrile in 1 min and held for 15 min. The injection sample volume was 20 μL, and UV detection wavelength was 225 nm.

Adsorption experiments

The adsorption experiments were carried out in 25-mL glass bottles with the following procedures. Firstly, 100 mg of composite material was added to 10 mL of PAEs solution (pH 6–7) and shaken for 40 min at 25 °C. Then the material was isolated from the solution using a permanent magnet, and PAEs concentrations in the solution before and after adsorption were determined. The adsorption efficiency (α) and adsorption capacity Q (mg·g-1) were calculated according to the following equations:

$$\alpha = \frac{C_0 - C_e}{C_0} \times 100\% \quad (1)$$

$$Q = \frac{(C_0 - C_e)V}{m} \quad (2)$$

where C_0 (mg·L^{-1}) and C_e (mg·L^{-1}) are the initial and equilibrium concentrations of the three PAEs, respectively; V (mL) is solution volume; m (mg) is adsorbent mass.

To determine the effect of pH, the initial pH of the solution containing 5 mg L^{-1} PAEs was adjusted from 3.0 to 11.0 by using 0.1 mol L^{-1} HCl and 0.1 mol L^{-1} NaOH as needed. For the assessment of kinetic performance, 10 mL of 5 mg L^{-1} PAEs solution was used, and the adsorbent amount was fixed at 100 mg. At different time intervals, the adsorbent was isolated by a magnet, and the supernatant was measured by HPLC. In case of maximum adsorption capacities of mag-MMIP@MWCNTs to the three PAEs, the adsorption isotherms were studied based on different PAEs initial concentrations when the other conditions were fixed. To investigate the influence of temperature and further analyze the adsorption mechanisms, the initial concentration of PAEs was fixed at 5 mg L^{-1} and the temperature was varied from 10 °C to 40 °C. The selectivity of mag-MMIP@MWCNTs was performed in 10 mL of mixed solution containing 5 mg L^{-1} DMP, DEP, DBP, DEHP, and H_2PA by using mag-NIP@MWCNTs as contrast.

Evaluation of the reusability and reproducibility

To evaluate the reusability, 100 mg of newly prepared composite was added into 10 mL of 5 mg L^{-1} three PAEs solution and shaken at 25 °C for 40 min. Then, the composite was isolated by a magnet and washed with 10% acetic acid in methanol (v/v) for several times until no PAEs detected, and washed to be neutral with ethanol, dried under vacuum at 60 °C. After desorption, the composite was reused for several cycles to estimate the reusability as a potential material in real performance. The reproducibility was investigated using the composites prepared in three different batches.

Adsorption of PAEs spiked in environmental water samples

The surface water, groundwater, and domestic sewage samples (no DMP, DEP, and DBP detected) were collected from Bishan, Nanchuan, and Xiushan (Chongqing, China), respectively. The environmental water samples were passed through a 0.45-μm polypropylene film, and the three PAEs (5 mg L^{-1}) were spiked in the filtrates. Mag-MMIP@MWCNTs (100 mg) was added to 10 mL of the spiked environmental water sample, and then the adsorption and detection procedures were carried out as described in the adsorption experiment.

Results and discussion

Preparation and characterization of mag-MMIP@MWCNTs

The preparation of mag-MMIP@MWCNTs involved the preparation of MWCNTs@Fe_3O_4, silica shell modified on the surface of MWCNTs@Fe_3O_4, MIPs layer functionalized onto the composite, and final formation of recognition sites on the imprinting composite. Firstly, the negatively charged MWCNTs-COOH was formed by treating MWCNTs under acidic condition, which was beneficial for electrostatic attraction between MWCNTs and iron ions in the system to successfully introduce Fe_3O_4 particles onto the surface of MWCNTs through hydrothermal reaction, and thus provided a "magnetic core" for the material. In order to prevent the oxidation of magnetic core and increase the efficient combination of "core" and MIPs, the double bond modified silicon shell was then coated on MWCNTs@Fe_3O_4 by sol-gel and surface grafting techniques (Guo et al. 2015). Finally, MWCNTs@Fe_3O_4@SiO_2-C=C was mixed with DMP, DEP, and DBP (multiple-template molecules), MAA (functional monomer), EGDMA (cross linker), and AIBN (initiator), then the mixture were reacted to form the printing layer of PAEs through thermal polymerization, and thus the MIP was loaded on MWCNTs@Fe_3O_4@SiO_2-C=C by covalent coupling. After elution, specific recognition sites were formed on the imprinting layer.

SEM images of the prepared materials at different stages are shown in Fig. S1 (Supplementary Material). It can be seen that MWCNTs with the diameter of 60–100 nm are tubular structure and intertwined (Fig. S1a), which provide the

framework support for the core-shell magnetic MIP in this study. The morphology of carbon nanotubes does not change obviously, and Fe_3O_4 nanoparticles with the mean diameter of about 200 nm are well distributed on the surface of MWCNTs in MWCNTs@Fe_3O_4 (Fig. S1b), which confirms that the "magnetic core" has been successfully modified to give MWCNTs magnetic property. After silicon coating modification, the thickness of Fe_3O_4 nanoparticles in MWCNTs@Fe_3O_4@SiO_2 increases to about 350 nm (Fig. S1c), and Fe_3O_4 nanoparticles become smoother than those in MWCNTs@Fe_3O_4 (Fig. S1b). Finally, the thickness of the nanoparticles increases to about 400 nm, and corresponds to a 50-nm thick MIP layer covered on magnetic nanoparticles in MWCNTs@Fe_3O_4@SiO_2-C=C (Fig. S1d), which may be beneficial for mass transfer between the solution and mag-MMIP@MWCNTs, and improves the incomplete template removal caused by "deep buried" binding sites (Figueiredo et al. 2016).

FTIR spectra of the prepared materials at different stages are shown in Fig. S2 (Supplementary Material). For MWCNTs (curve a), no obvious characteristic peaks can be observed. In FTIR spectra of MWCNTs@Fe_3O_4 (curve b), MWCNTs@Fe_3O_4@SiO_2 (curve c) and MWCNTs@Fe_3O_4@SiO_2-C=C (curve d), the characteristic absorption peaks of Fe–O stretching vibration are all observed at 577 cm^{-1} or 573 cm^{-1}, which give a further evidence that Fe_3O_4 nanoparticles have been successfully loaded on the surface of MWCNTs. The absorption peaks at 1076 cm^{-1}, 801 cm^{-1} (or 793 cm^{-1}), and 462 cm^{-1} are ascribed to asymmetric stretching vibration, symmetric stretching vibration and bending vibration of Si-O-Si, and those at 3450 cm^{-1} and 1645 cm^{-1} are attributed to stretching vibration and bending vibration of O-H, respectively. The characteristic peak at 2926 cm^{-1} is the stretching vibration peak of C–H bonds on methyl and methylene, which can be ascribed to KH-570 modification on silica shell (Wu et al. 2016). The existence of these characteristic peaks indicates that the modified silica shell has been successfully loaded on the surface of MWCNTs@Fe_3O_4.

The magnetic property of the prepared materials was investigated by vibrating sample magnetometer. As seen in Fig. S3 (Supplementary Material), the magnetic hysteresis loops of MWCNTs@Fe_3O_4, MWCNTs@Fe_3O_4@SiO_2, and mag-MMIP@MWCNTs have similar shape (Fig. S3a), and their saturation magnetization values are 66.25, 36.66, and 25.6 emu g^{-1}, respectively. According to the view of Ma et al. (Ma et al. 2005), the saturation magnetization of mag-MMIP@MWCNTs is lower than that of MWCNTs@Fe_3O_4 owing to the encapsulation of silica and PAEs imprinting layer, but the magnetism of mag-MMIP@MWCNTs is sufficient for magnetic separation using an external magnet. Moreover, the remanent magnetization and coercive force of three materials are close to zero, indicating that they have superparamagnetism, and thus enable rapid dispersion after removing the magnetic field (Gao et al. 2014). In Fig. S3b, the black homogeneous dispersion of mag-MMIP@MWCNTs is observed in the absence of an external magnetic field, and the composite can be quickly and completely isolated from the dispersion by placing an external magnet near the glass vial.

The surface area and porosity of mag-MMIP@MWCNTs and mag-NIP@MWCNTs were measured by BET analysis, and the N_2 adsorption-desorption isotherms are shown in Fig. S4 (Supplementary Material). The adsorption-desorption curves can be identified as type IV hysteresis loop according to the IUPAC classification, indicating that both mag-MMIP@MWCNTs and mag-NIP@MWCNTs are mesoporous materials. The specific surface area and pore volume of mag-MMIP@MWCNTs are slightly higher than those of mag-NIP@MWCNTs, suggesting that the former is more suitable for the binding of the three PAEs (Li et al. 2009). From another perspective, the different adsorption properties of mag-MMIP@MWCNTs and mag-NIP@MWCNTs cannot be completely attributed to the differences in morphology, which are related to specific recognition sites in molecular imprinting process (Mao et al. 2016).

Effect of solution pH

Figure 2 shows the effect of solution pH on the adsorption efficiency. As we can see, the removal efficiencies are relatively low at pH 3, and slightly increase and keep stable when solution pH changes from 5 to 9 for every PAE, and then have a significant increase at pH 11 for DMP and DEP. In fact, OH^- in solution can easily induce PAEs hydrolysis under alkaline condition, so the removal efficiency at pH 11 cannot truly reflect the adsorption capability of mag-MMIP@MWCNTs to the three PAEs. The adsorption properties of mag-

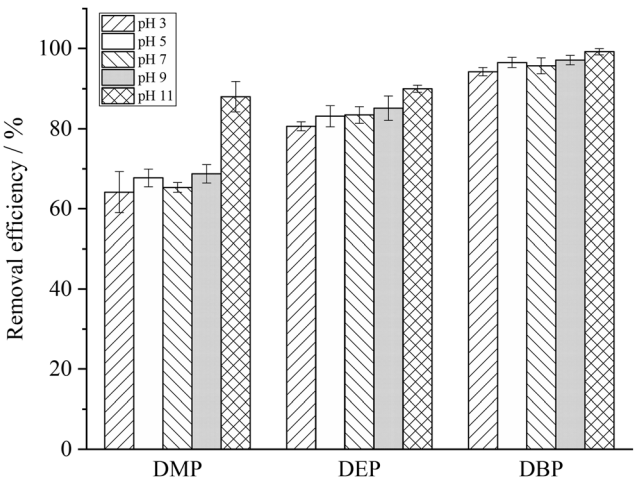

Fig. 2 Effect of solution pH on the adsorption of mag-MMIPs@MWCNTs to the three PAEs. (PAEs initial concentrations: 5 mg L^{-1}; adsorption time: 40 min; temperature: 25 °C)

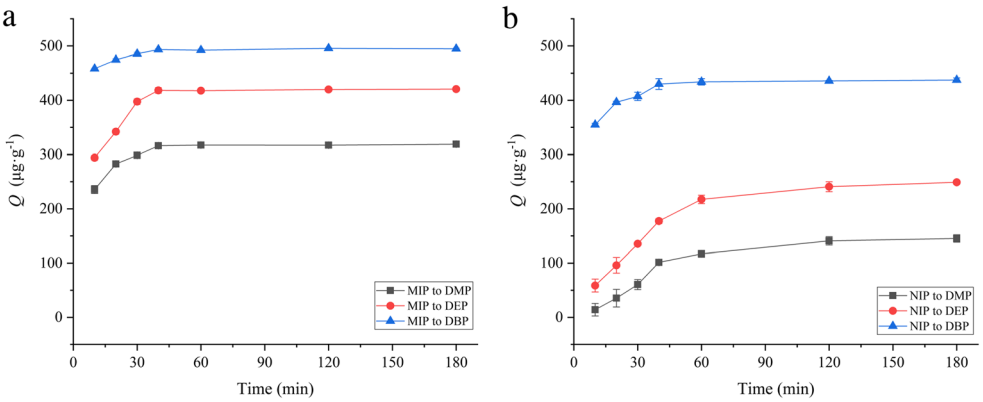

Fig. 3 Adsorption kinetic curves of mag-MMIPs@MWCNTs to the three PAEs (**a**) and mag-NIP@MWCNTs (**b**). (PAEs initial concentrations: 5 mg·L^{-1}; solution pH: 7; temperature: 25 °C)

MMIP@MWCNTs at pH 5 to 9 are favorable for the removal of the three PAEs in natural water, because the real pH of actual water environment is mostly distributed in this range. So we did not adjust the pH of adsorption solution in the following experiments.

Effect of contact time and adsorption kinetics

Contact time is an important parameter affecting the adsorption efficiency (Awual et al. 2019a). The dynamic binding curves of the three PAEs on mag-MMIP@MWCNTs and mag-NIP@MWCNTs were investigated at various time, and the results are shown in Fig. 3. It can be seen that the three PAEs on mag-MMIP@MWCNTs display similar dynamic binding curves (Fig. 3a), and they can rapidly transfer and occupy enough binding sites on the material surface in the first 30 min, and thus the adsorption rates increase rapidly. With the decrease of binding sites, the adsorption rates slow down and the adsorption capacities gradually tend to be constant at 40 min. Compared with the traditional bulk polymers, mag-MMIP@MWCNTs with nano-sized imprinting layer can effectively improve mass transfer and thus greatly shorten the adsorption time (He et al. 2010; Wolska and Bryjak 2012). Because of the hydrophobicity of the three PAEs and π-π interaction between PAEs (π-acceptor) and MWCNTs (π-donor) (Julinová and Slavík 2012; Wang et al. 2010), mag-NIP@MWCNTs can also adsorb the three PAEs (Fig. 3b), but it need more time (about 60 min) to reach adsorption equilibrium. Compared with DMP and DEP, DBP has higher octanol-water partition coefficient, thus stronger hydrophobicity makes it easy to be adsorbed, so the adsorption capacity displays an increasing order of DMP, DEP and DBP. During the preparation of mag-MIP@MWCNTs, the three PAEs was used as template molecules to create the tailor-made binding sites, the adsorption capacities of the three PAEs on mag-MIP@MWCNTs are much higher than those on mag-NIP@MWCNTs under the same conditions. Based on these results, 40 min was chosen as the adsorption time for the adsorption of mag-MMIP@MWCNTs to the three PAEs.

To study the kinetic characteristics of adsorption process, the experimental data were fitted by pseudo first-order, pseudo second-order and intraparticle diffusion kinetic models, and the results are shown in Table 1. The highest determination coefficients (R^2) can be obtained by pseudo second-order kinetic model for the adsorption of the three PAEs, and the equilibrium adsorption capacities ($Q_{2e,\ fitted}$) of DMP, DEP and DBP are close to the experimental values. In addition, the good linear relationship between t/Q_t and t implies that the rate-limiting step might be governed by the occupation of the binding sites by PAEs through noncovalent interaction (Guo et al. 2019; Qian et al. 2017).

Table 1 Adsorption kinetic parameters of mag-MIP@MWCNTs to DMP, DEP and DBP

Compound	Pseudo first-order kinetic model $\ln(Q_e - Q_t) = \ln Q_e - k_1 t$			Pseudo second-order kinetic model $\frac{t}{Q_t} = \frac{1}{k_2 Q_e^2} + \frac{t}{Q_e}$			Intraparticle diffusion model $Q_t = k_3 t^{0.5} + c$		
	$Q_{1e,\ fitted}$ (μg·g^{-1})	k_1 (min^{-1})	R^2	$Q_{2e,\ fitted}$ (μg·g^{-1})	k_2 (mg·μg^{-1}·min^{-1})	R^2	c	k_3 (μg·g^{-1}·min$^{-0.5}$)	R^2
DMP	79.66	0.060	0.8761	303.0	2.86	0.9998	256.37	4.38	0.4321
DEP	108.2	0.053	0.7673	416.7	1.28	0.9994	317.38	8.41	0.4861
DBP	134.0	0.081	0.7962	500.0	4.41	0.9999	464.42	2.46	0.5523

Q_e and Q_t are the adsorption capacities at equilibrium and t time, $Q_{1e,\ fitted}$ and $Q_{2e,\ fitted}$ are the adsorption capacities fitted by pseudo first-order and second-order kinetic models, respectively. k_1, k_2, and k_3 are pseudo first-order, second-order and intraparticle diffusion rate constants, respectively. c is a constant for boundary layer thickness

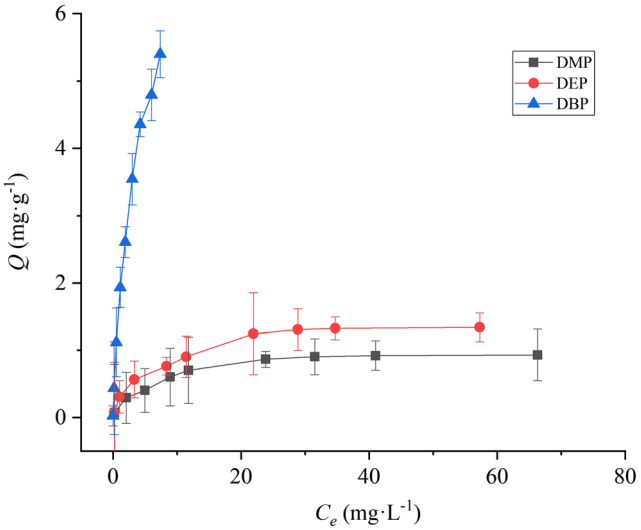

Fig. 4 Adsorption isotherms of mag-MMIP@MWCNTs to the three PAEs. (solution pH: 7; adsorption time: 40 min; temperature: 25 °C)

PAEs initial concentration and adsorption isotherms

To determine the maximum adsorption capacities, the isothermal adsorption experiments were conducted at different PAEs initial concentrations, and the results are shown in Fig. 4. Apparently, the adsorption capacities of DMP and DEP increase with the initial concentration increasing, and tend to be constant when higher than 30 mg L^{-1}. However, the adsorption capacity of DBP increases rapidly with the initial concentration, and the adsorption does not reach equilibrium in the investigated concentration range, implying that mag-MMIP@MWCNTs has higher adsorption ability for DBP. Overall, mag-MMIP@MWCNTs is more effective to adsorb DMP and DEP not exceeding 30 mg L^{-1}, and has a good applicability for DBP from low to high concentrations.

The adsorption isotherms were assessed by the Langmuir and Freundlich isothermal adsorption models, and the results are shown in Table 2. Overall, Langmuir model can describe the adsorption processes of DBP, DEP, and DMP very well, and the maximum adsorption capacities (Q_{max}) are obtained as 7.09, 1.38, and 0.95 mg g^{-1}, respectively. The high determination coefficients of Langmuir model indicate that the adsorption of DMP and DEP on mag-MMIPs@MWCNTs is monolayer adsorption, which mainly occur on the specific or active binding sites of the imprinted layer and the surface of adsorbent (Kong et al. 2012). Due to the binding sites of the imprinted layer and the interaction of DBP and MWCNTs, the adsorption of DBP is inclined to heterogeneous adsorption (Wang et al. 2010). A comparison of PAEs adsorption with other functional materials has been made and the data are summarized in Table 3. Mag-MMIP@MWCNTs has high adsorption capacity with shorter adsorption time, and can simultaneously adsorb DMP, DEP, and DBP in aqueous solution.

In order to further investigate the binding properties of mag-MMIP@MWCNTs to the three PAEs, the Scatchard analysis was adopted to evaluate adsorption parameters (Zhang et al. 2018):

$$\frac{Q}{C_e} = \frac{Q_{max}}{K_d} - \frac{Q}{K_d} \quad (3)$$

where Q is the adsorbate amount bound to adsorbent (mg·g^{-1}); Q_{max} is apparent maximum binding amount (mg·g^{-1}); C_e (mg·L^{-1}) is the equilibrium concentration of adsorbate; K_d is the dissociation constant of binding sites.

The relationship between Q/C_e and Q was fitted to two distinct linear equations, indicating that there are probably two classes of binding sites for the adsorption of mag-MMIP@MWCNTs to the three PAEs, i.e., specific binding sites with high affinity and unspecific binding sites with low affinity (Table 4). The K_d and Q_{max} values of two classes of binding sites can be obtained from the slope and intercept of the Scatchard plot at adsorption equilibrium, respectively. Compared with the two groups of $1/K_d$, the binding affinities of high affinity sites for DMP, DEP, and DBP are 4.8, 2.7, and 2.9 times higher than those of low affinity sites, respectively. However, the Q_{max} values of high affinity sites are lower than those of low affinity sites, suggesting that the adsorption processes result from the combination of two kinds of binding

Table 2 Fitted results of the isothermal adsorption of mag-MMIP@MWCNTs to DMP, DEP, and DBP by Langmuir and Freundlich models

Compound	Langmuir model				Freundlich model			
	$\frac{C_e}{Q} = \frac{C_e}{Q_{max}} + \frac{1}{K_L}$	Q_{max} (mg·g^{-1})	K_L	R^2	$\lg Q = \lg K_F + \frac{1}{n}\lg C_e$	K_F	$1/n$	R^2
DMP	$y = 1.05x + 4.78$	0.95	0.22	0.994	$y = 0.43x - 0.72$	0.19	0.43	0.935
DEP	$y = 0.72x + 3.15$	1.38	0.23	0.992	$y = 0.47x - 0.57$	0.27	0.47	0.943
DBP	$y = 0.14x + 0.37$	7.09	0.38	0.976	$y = 0.77x + 0.18$	1.52	0.77	0.984

C_e (mg·L^{-1}) is the equilibrium concentration of adsorbate; Q is adsorption capacity; Q_{max} is the maximum adsorption capacity; n is an empirical constant related to the adsorption intensity; K_L and K_F are Langmuir and Freundlich adsorption equilibrium constants, respectively

Table 3 Comparison of PAEs adsorption with other functional materials

Adsorbent	Compound	Q_{max} (mg·g^{-1})	Equilibrium time	Reference
Mesoporous-ordered carbon	DBP	0.209	1 h	(Jedynak et al. 2017)
Pepper straw biochars (400 °C)	DMP	1.773	144 h	(Yao et al. 2019)
	DBP	6.292	96 h	
α-Cyclodextrin-linked chitosan bead	DEP	2.82	6 h	(Chen et al. 2007)
Coal-chitosan composite	DEP	42.67	4 h	(Shaida et al. 2018)
K-mont clay	DEP	1.89	120 h	(Wu et al. 2015)
Biochar-graphene nanosheet	DMP	12.21	48 h	(Abdul et al. 2017)
	DEP	10.04		
	DBP	5.43		
Molecularly imprinted microspheres	DBP	0.737	12 h	(He et al. 2010)
GO-MNPs	DEP	8.71	5 min	(Yin et al. 2014)
MGO@mSiO$_2$-MIP	DMP, DEP, DBP, BBP, DEHP, DOP	2.3-4.8	2 h	(Guo et al. 2019)
Mag-MMIP@MWCNTs	DMP, DEP, DBP	9.42	40 min	This work

sites, and are mainly dependent on physical adsorption of unspecific binding (Pan et al. 2011).

Effect of temperature and adsorption mechanisms

The influence of temperature on the adsorption of mag-MMIP@MWCNTs to the three PAEs was investigated, and the results are shown in Fig. 5. It can be seen that the adsorption capacity shows a decreasing trend with the temperature increasing. The adsorption capacities of DMP, DEP, and DBP are 364.1, 444.8, and 505.6 μg g^{-1} at 10 °C, and those were reduced to 254.3, 348.9, and 467.6 μg g^{-1} at 40 °C, respectively. These results indicate that the relative low temperature is beneficial for the adsorption of the three PAEs.

In order to further study adsorption thermodynamic behaviors, the following equations were introduced (Wang et al. 2010):

$$\ln K_D = \frac{\Delta S}{R} - \frac{\Delta H}{RT} \quad (4)$$

$$\Delta H = \Delta G + T\Delta S \quad (5)$$

where K_D represents adsorption distribution coefficient calculated by the ratio of the adsorbate amounts in solid phase and liquid phase at adsorption equilibrium; R is the universal gas constant (8.314 J·mol^{-1} K^{-1}), and T is thermodynamic temperature (K); ΔG, ΔH, and ΔS are Gibbs free energy change (kJ·mol^{-1}), enthalpy change (kJ·mol^{-1}), and entropy change (J·mol^{-1}·K^{-1}), respectively.

The adsorption thermodynamic parameters are shown in Table 5. It can be seen that ΔG and ΔH values are negative, suggesting that the adsorption processes are spontaneous and exothermic, and K_D values decrease with the increase of temperature. ΔG and ΔH values display a decreasing order of DBP, DEP, and DMP at every temperature, indicating that low temperature is beneficial for the adsorption process, and DBP has the strongest migration ability from solution to the composite surface. Meanwhile, the negative ΔS values correspond to the decreases in the degree of freedom at solid-liquid interface during the adsorption processes. In general, ΔG value is in the range of − 20 to 0 kJ mol^{-1} with ΔH of − 40 to 20 kJ mol^{-1} for physical adsorption, while ΔG value is in the range of − 400 to − 80 kJ mol^{-1} for chemical adsorption (Ren et al. 2015; Sharma et al. 2013). Based on the viewpoint of von Oepen et al. (von Oepen et al. 1991), the absolute values of adsorption ΔH caused by hydrogen bond, van der Waals force, and hydrophobic interaction are 2–40, 4–10, and 5 kJ mol^{-1}, respectively. Therefore, the adsorption of mag-

Table 4 The Scatchard analysis of the adsorption of mag-MMIPs@MWCNTs to DMP, DEP, and DBP

Compound	High affinity sites			Low affinity sites		
	Linear equation	K_d	Q_{max}	Linear equation	K_d	Q_{max}
DMP	$y = -0.64x + 0.34$	1.55	0.52	$y = -0.13x + 0.13$	7.42	0.94
DEP	$y = -0.49x + 0.46$	2.03	0.94	$y = -0.18x + 0.26$	5.42	1.42
DBP	$y = -0.77x + 3.14$	1.30	4.08	$y = -0.26x + 2.13$	3.79	8.09

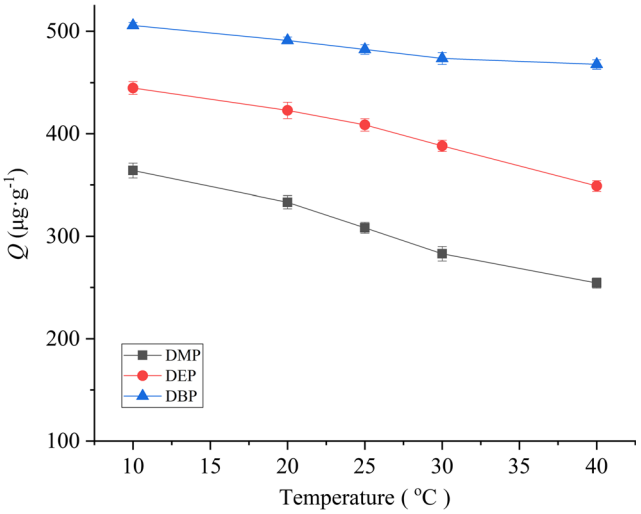

Fig. 5 Effect of temperature on the adsorption of mag-MMIPs@MWCNTs to the three PAEs. (PAEs initial concentrations: 5 mg L^{-1}; adsorption time: 40 min; solution pH 7)

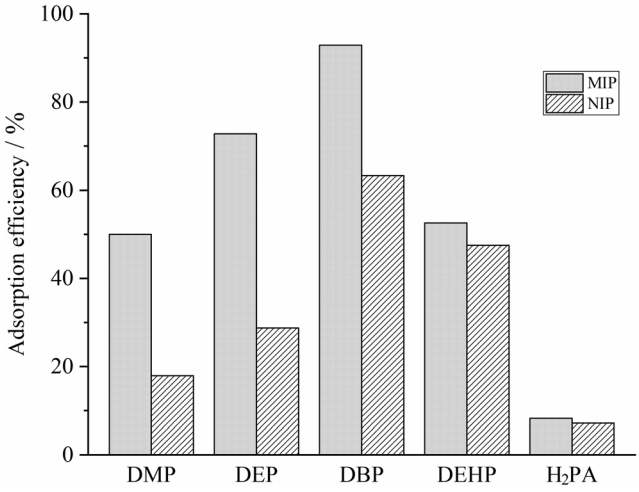

Fig. 6 The selectivity of mag-MMIP@MWCNTs and mag-NIP@MWCNTs. (The initial concentrations of DMP, DEP, DBP, DEHP and H_2PA: 5 mg L^{-1}; solution pH: 7; adsorption time: 40 min; temperature: 25 °C)

MMIP@MWCNTs to the three PAEs is dominated by physical process, and mainly relying on hydrogen bond between PAEs and MAA, hydrophobic interaction and van der Waals force between MWCNTs and PAEs (Zhang et al. 2018).

Adsorption selectivity of mag-MMIP@MWCNTs

In order to examine the adsorption selectivity of mag-MMIP@MWCNTs, DEHP, and H_2PA were selected as analogues and mag-NIP@MWCNTs was used as contrast. The selective adsorption of these analogues is shown in Fig. 6. The results indicate that the adsorption capacities of DMP, DEP, and DBP on mag-MMIP@MWCNTs are evidently higher than those on mag-NIP@MWCNTs, which are similar to the results of adsorption kinetic experiments. However, due to the deficiency of bonding sites on the surface of mag-MMIP@MWCNTs, the adsorption capacities of DEHP and H_2PA on mag-MMIP@MWCNTs are close to those observed on mag-NIP@MWCNTs. The imprinting factor is usually used to evaluate the specific recognition property of imprinted material to template molecules and structurally similar compounds. According to the ratios of adsorption capacity of the five compounds on mag-MMIP@MWCNTs to that on mag-NIP@MWCNTs, the imprinting factors of DMP, DEP, DBP, DEHP, and H_2PA can be obtained as 2.79, 2.53, 1.54, 1.12, and 1.15, respectively. The imprinting factors of DMP, DEP

Table 5 Adsorption thermodynamic constants of mag-MMIP@MWCNTs to DMP, DEP, and DBP

Compound	T (K)	lnK_D	ΔG (kJ·mol^{-1})	ΔH (kJ·mol^{-1})	ΔS (J·mol^{-1}·K^{-1})
DMP	283	5.59	− 13.15	− 24.15	− 38.83
	293	5.30	− 12.90		
	298	5.08	− 12.59		
	303	4.87	− 12.27		
	313	4.64	− 12.07		
DEP	283	6.69	− 15.74	− 31.04	− 53.31
	293	6.31	− 15.36		
	298	6.10	− 15.12		
	303	5.85	− 14.74		
	313	5.44	− 14.16		
DBP	283	8.68	− 20.41	− 41.85	− 77.32
	293	7.96	− 19.40		
	298	7.70	− 19.08		
	303	7.33	− 18.48		
	313	6.98	− 18.17		

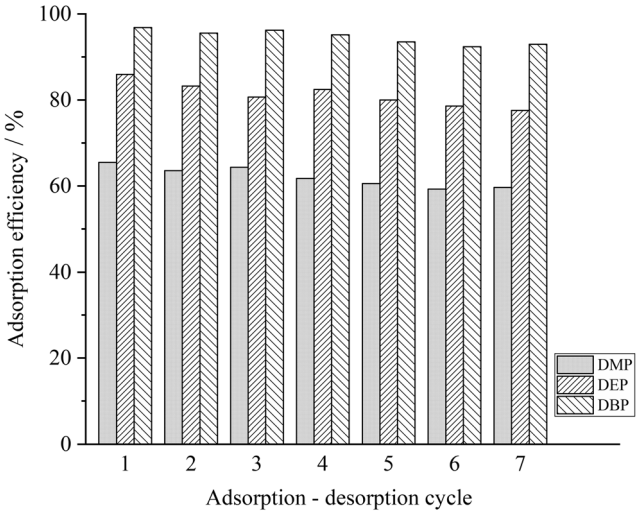

Fig. 7 Reusability of mag-MMIP@MWCNTs

and DBP are higher than those of DEHP and H_2PA, suggesting that mag-MMIP@MWCNTs has a relatively high affinity for the template molecules. These results illustrate that the obtained mag-MMIP@MWCNTs exhibit adsorption selectivity for DMP, DEP, and DBP.

Reproducibility and reusability of mag-MMIP@MWCNTs

The reproducibility and reusability of mag-MMIP@MWCNTs were investigated using the composites prepared in three batches and the same batch, respectively. For the three-batch composites, the relative standard deviations (RSDs) of adsorption efficiency were obtained as 1.4–5.7%, further implying that mag-MMIP@MWCNTs can be prepared repeatedly. The elution, regeneration and subsequent reuse are very important to evaluate the sustainable application and cost-effectiveness of the adsorbent (Awual et al. 2016). After seven adsorption-desorption cycles of the same batch composites, the adsorption efficiencies of DMP, DEP, and DBP are 59.7%, 77.6%, and 92.9% (Fig. 7), which still maintain at 91.1%, 90.4%, and 95.4% of the initial adsorption efficiencies, respectively. These results indicate that mag-MMIP@MWCNTs has good stability and can be reused to adsorb the three PAEs after regeneration. The slight decreases of adsorption capacity may be due to the blocking of some recognition sites by template molecules or the slight destruction by multiple elution during the reuse of mag-MMIP@MWCNTs.

Adsorption of PAEs spiked in environmental water samples

In order to inspect the feasibility of adsorbent for PAEs removal, mag-MMIP@MWCNTs was applied to adsorb the three PAEs spiked in environmental water samples, and the removal efficiencies are shown in Table 6. The results indicate that the three PAEs can be effectively removed by mag-MMIP@MWCNTs, and testify that this composite is a promising adsorbent for rapid and efficient removal of PAEs in environmental water samples.

Conclusions

Combined magnetic surface imprinting technique with multi-template imprinting strategy, a novel magnetic core-shell structured multi-template molecularly imprinted polymer based on MWCNTs (mag-MMIP@MWCNTs) has been successfully prepared and used for the simultaneous adsorption of DMP, DEP, and DBP in aqueous solution. This composite can not only recognize the three PAEs with high selectivity, but also display favorable reproducibility and reusability, and good magnetic separation performance. The adsorption processes of the three PAEs were well described by pseudo second-order kinetic model, and the isothermal adsorption data were well fitted by Langmuir model with maximum adsorption capacities of 0.95, 1.38, and 7.09 mg g^{-1} for DMP, DEP and DBP, respectively. Relying on hydrogen bond, hydrophobic interaction, and the van der Waals force, the adsorption of the three PAEs is a spontaneous and endothermic process. Moreover, this composite has high adsorption capacity with shorter adsorption time, and has been successfully applied to simultaneous removal of the three PAEs spiked in environmental water samples. Mag-MMIP@MWCNTs has a great potential to effectively remove multiple PAEs and protect aquatic ecological environment.

Table 6 Removal efficiencies of DMP, DEP, and DBP spiked in environmental water samples

Water sample	Spiked concentration	Removal efficiency (%)		
		DMP	DEP	DBP
Groundwater	5 mg L^{-1}	60.0 ± 7.2	74.6 ± 4.8	94.1 ± 3.4
Surface water		66.3 ± 6.7	84.0 ± 4.0	96.9 ± 1.1
Domestic sewage		51.4 ± 7.7	75.4 ± 6.1	94.7 ± 2.6

Availability of data and materials All data generated or analyzed during this study are included in this published article and its supplementary information files.

Authors' contributions Dongli Deng and Jinzhong Zhang contributed to the study conception and design. Material preparation and data collection and analysis were performed by Dongli Deng, Yingnan He, Mingyuan Li, and Ludan Huang. The first draft of the manuscript was written by Dongli Deng and all authors commented on previous version of the manuscript. Jinzhong Zhang participated in the analysis with constructive discussions. All authors read and approved the final manuscript.

Funding National Key Research and Development Program of China (No. 2018YFD0800601), Chongqing Key Research & Development Program of Technology Innovation and Application Demonstration (cstc2018jszx-zdyfxmX0002), Science and Technology Research Program of Chongqing Education Commission of China (No. KJ1503107), and Science and Technology Research Program of Chongqing Industry Polytechnic College (No. GZY201707).

Compliance with ethical standards

Conflict of interest The authors declare that they have no competing interests.

References

Abdel daiem MM, Rivera-Utrilla J, Ocampo-Perez R, Mendez-Díaz JD, Sanchez-Polo M (2012) Environmental impact of phthalic acid esters and their removal from water and sediments by different technologies-a review. J Environ Manag 109:164–178

Abdul G, Wang P, Zhang D, Li H (2015) Adsorption of diethyl phthalate on carbon nanotubes: pH dependence and thermodynamics. Environ Eng Sci 32:103–110

Abdul G, Zhu XY, Chen BL (2017) Structural characteristics of biochar-graphene nanosheet composites and their adsorption performance for phthalic acid esters. Chem Eng J 319:9–20

Awual MR, Hasan MM, Khaleque MA, Sheikh MC (2016) Treatment of copper(II) containing wastewater by a newly developed ligand based facial conjugate materials. Chem Eng J 288:368–376

Awual MR, Hasan MM, Asiri AM, Rahman MM (2019a) Cleaning the arsenic(V) contaminated water for safe-guarding the public health using novel composite material. Compos B Eng 171:294–301

Awual MR, Hasan MM, Rahman MM, Asiri AM (2019b) Novel composite material for selective copper(II) detection and removal from aqueous media. J Mol Liq 283:772–780

Chen WL, Sung HH (2005) The toxic effect of phthalate esters on immune responses of giant freshwater prawn (*Macrobrachium rosenbergii*) via oral treatment. Aquat Toxicol 74:160–171

Chen CY, Chen CC, Chung YC (2007) Removal of phthalate esters by α-cyclodextrin-linked chitosan bead. Bioresour Technol 98:2578–2583

Chen LX, Wang XY, Lu WH, Wu XQ, Li JH (2016) Molecular imprinting: perspectives and applications. Chem Soc Rev 45:2137–2211

Ding MY, Kang QY, Zhang SY, Zhao FR, Zhang HF, Yang M, Hu JY (2019) National survey of phthalate metabolites in drinking source water of 23 cities in China. China Environ Sci 39:4205–4211 (in Chinese)

Fang ZQ, Huang HJ (2010) Adsorption of di-n-butyl phthalate onto nutshell-based activated carbon. Equilibrium, kinetics and thermodynamics. Adsorpt Sci Technol 27:685–700

Figueiredo L, Erny GL, Santos L, Alves A (2016) Applications of molecularly imprinted polymers to the analysis and removal of personal care products: a review. Talanta 146:754–765

Gani KM, Kazmi AA (2016) Phthalate contamination in aquatic environment: a critical review of the process factors that influence their removal in conventional and advanced wastewater treatment. Crit Rev Environ Sci Technol 46:1402–1439

Gani KM, Tyagi VK, Kazmi AA (2017) Occurrence of phthalates in aquatic environment and their removal during wastewater treatment processes: a review. Environ Sci Pollut Res 24:17267–17284

Gao C, Guo Z, Liu JH, Huang XJ (2012) The new age of carbon nanotubes: an updated review of functionalized carbon nanotubes in electrochemical sensors. Nanoscale 4:1948–1963

Gao RX, Hao Y, Zhao SQ, Zhang LL, Cui XH, Liu DC, Tang YH, Zhang YS (2014) Novel magnetic multi-template molecularly imprinted polymers for specific separation and determination of three endocrine disrupting compounds simultaneously in environmental water samples. RSC Adv 4:56798–56808

Guo XY, Mao FF, Wang WJ, Yang Y, Bai ZM (2015) Sulfhydryl-modified Fe_3O_4@SiO_2 core/shell nanocomposite: synthesis and toxicity assessment in vitro. ACS Appl Mater Interfaces 7:14983–14991

Guo LH, Ma XG, Xie XW, Huang RF, Zhang MY, Li J, Zeng GL, Fan YM (2019) Preparation of dual-dummy-template molecularly imprinted polymers coated magnetic graphene oxide for separation and enrichment of phthalate esters in water. Chem Eng J 361:245–255

He J, Lv RH, Cheng J, Li YX, Xue JF, Lu K, Wang FC (2010) Preparation and characterization of molecularly imprinted microspheres for dibutyl phthalate recognition in aqueous environment. J Sep Sci 33:3409–3414

Huang DL, Wang RZ, Liu YG, Zeng GM, Lai C, Xu P, Lu BA, Xu JJ, Wang C, Huang C (2015) Application of molecularly imprinted polymers in wastewater treatment: a review. Environ Sci Pollut Res 22:963–977

Jedynak K, Wideł D, Oszczudłowski J (2017) Removal of selected phthalates from aqueous solution by mesoporous-ordered carbon adsorbent. Adsorpt Sci Technol 35:744–750

Julinová M, Slavík R (2012) Removal of phthalates from aqueous solution by different adsorbents: a short review. J Environ Manag 94:13–24

Khan NA, Jung BK, Hasan Z, Jhung SH (2015) Adsorption and removal of phthalic acid and diethyl phthalate from water with zeolitic imidazolate and metal-organic frameworks. J Hazard Mater 282:194–200

Kong X, Gao RX, He XW, Chen LX, Zhang YK (2012) Synthesis and characterization of the core-shell magnetic molecularly imprinted polymers (Fe_3O_4@MIPs) adsorbents for effective extraction and determination of sulfonamides in the poultry feed. J Chromatogr A 1245:8–16

Kumar N, Narayanan N, Gupta S (2018) Application of magnetic molecularly imprinted polymers for extraction of imidacloprid from eggplant and honey. Food Chem 255:81–88

Li Y, Li X, Li YQ, Qi JY, Bian J, Yuan YX (2009) Selective removal of 2,4-dichlorophenol from contaminated water using non-covalent imprinted microspheres. Environ Pollut 157:1879–1885

Li X, Ma XG, Huang RF, Xie XW, Guo LH, Zhang MY (2018) Synthesis of a molecularly imprinted polymer on mSiO_2@Fe_3O_4 for the selective adsorption of atrazine. J Sep Sci 41:2837–2845

Liu XW, Shi JH, Bo T, Zhang H, Wu W, Chen QC, Zhan XM (2014) Occurrence of phthalic acid esters in source waters: a nationwide survey in China during the period of 2009-2012. Environ Pollut 184:262–270

Lu WH, Wang XY, Wu XQ, Liu DY, Li JH, Chen LX, Zhang XS (2017) Multi-template imprinted polymers for simultaneous selective solid-phase extraction of six phenolic compounds in water samples

followed by determination using capillary electrophoresis. J Chromatogr A 1483:30–39

Luo B, Song XJ, Zhang F, Xia A, Yang WL, Hu JH, Wang CC (2010) Multi-functional thermosensitive composite microspheres with high magnetic susceptibility based on magnetite colloidal nanoparticle clusters. Langmuir 26:1674–1679

Ma ZY, Guan YP, Liu HZ (2005) Synthesis and characterization of micron-sized monodisperse superparamagnetic polymer particles with amino groups. J Polym Sci A 43:3433–3439

Madikizela LM, Chimuka L (2016) Determination of ibuprofen, naproxen and diclofenac in aqueous samples using a multi-template molecularly imprinted polymer as selective adsorbent for solid-phase extraction. J Pharm Biomed Anal 128:210–215

Mao YL, Niu YF, Wu JF, Kang HY, Li D, Wang XW (2016) Selective recognition of ciprofloxacin from aqueous solution by molecularly imprinted polymers based on magnetic illite. Chin J Anal Chem 44: 915–922 (in Chinese)

Net S, Sempéré R, Delmont A, Paluselli A, Ouddane B (2015) Occurrence, fate, behavior and ecotoxicological state of phthalates in different environmental matrices. Environ Sci Technol 49:4019–4035

Oca ML, Rubio L, Sarabia LA, Ortiz MC (2016) Dealing with the ubiquity of phthalates in the laboratory when determining plasticizers by gas chromatography/mass spectrometry and PARAFAC. J Chromatogr A 1464:124–140

Ostovan A, Ghaedi M, Arabi M, Yang Q, Li JH, Chen LX (2018) Hydrophilic multi-template molecularly imprinted biopolymers based on a green synthesis strategy for determination of b-family vitamins. ACS Appl Mater Interfaces 10:4140–4150

Pan JM, Xu LC, Dai JD, Li XX, Hang H, Huo PW, Li CX, Yan YS (2011) Magnetic molecularly imprinted polymers based on attapulgite/Fe_3O_4 particles for the selective recognition of 2, 4-dichlorophenol. Chem Eng J 174:68–75

Qian S, Zhu H, Xiong BL, Zheng GC, Zhang JZ, Xu WH (2017) Adsorption and desorption characteristics of endosulfan in two typical agricultural soils in southwest china. Environ Sci Pollut Res 24: 11493–11503

Rao W, Cai R, Yin YL, Long F, Zhang ZH (2014) Magnetic dummy molecularly imprinted polymers based on multi-walled carbon nanotubes for rapid selective solid-phase extraction of 4-nonylphenol in aqueous samples. Talanta 128:170–176

Ren G, Yu Y, Peng SF, Du YM, Shi L, Lu G, Li YM (2015) Adsorption of malachite green (MG) and lissamine rhodamine (LR) on natural and modified zeolite. Environ Chem 34:367–376 (in Chinese)

Shaida MA, Dutta RK, Sen AK (2018) Removal of diethyl phthalate via adsorption on mineral rich waste coal modified with chitosan. J Mol Liq 261:271–282

Sharma P, Hussain N, Borah DJ, Das MR (2013) Kinetics and adsorption behavior of the methyl blue at the graphene oxide/reduced graphene oxide nanosheet–water interface: a comparative study. J Chem Eng Data 58:3477–3488

von Oepen B, Kördel W, Klein W (1991) Sorption of nonpolar compounds to soils: process, measurements and experience with the applicability of the modified OECD-guideline 106. Chemosphere 22:285–304

Wang F, Yao J, Sun K, Xing BS (2010) Adsorption of dialkyl phthalate esters on carbon nanotubes. Environ Sci Technol 44:6985–6991

Wang B, Wang HX, Zhou W, Chen Y, Zhou Y, Jiang QW (2015) Urinary excretion of phthalate metabolites in school children of China: implication for cumulative risk assessment of phthalate exposure. Environ Sci Technol 49:1120–1129

Wolska J, Bryjak M (2012) Sorption of phthalates on molecularly imprinted polymers. Sep Sci Technol 47:1316–1321

Wu YH, Si YB, Zhou DM, Gao J (2015) Adsorption of diethyl phthalate ester to clay minerals. Chemosphere 119:690–696

Wu XQ, Wang XQ, Lu WH, Wang XR, Li JH, You HY, Xiong H, Chen LX (2016) Water-compatible temperature and magnetic dual-responsive molecularly imprinted polymers for recognition and extraction of bisphenol A. J Chromatogr A 1435:30–38

Xu ZW, Zhang WM, Pan BC, Lv L (2011) Treatment of aqueous diethyl phthalate by adsorption using a functional polymer resin. Environ Technol 32:145–153

Yang JL, Li YX, Wang Y, Ruan J, Zhang J, Sun CJ (2015) Recent advances in analysis of phthalate esters in foods. Trends Anal Chem 72:10–26

Yao S, Li XN, Cheng H, Zhang C, Bian YR, Jiang X, Song Y (2019) Resource utilization of a typical vegetable waste as biochars in removing phthalate acid esters from water: a sorption case study. Bioresour Technol 293:122081

Yin LL, Lin YX, Jia L (2014) Graphene oxide functionalized magnetic nanoparticles as adsorbents for removal of phthalate esters. Microchim Acta 181:957–965

Zhang XK, Sarmah AK, Bolan NS, He LZ, Lin XM, Che L, Tang CX, Wang HL (2016) Effect of aging process on adsorption of diethyl phthalate in soils amended with bamboo biochar. Chemosphere 142: 28–34

Zhang H, Fang DL, Kong ZY, Wei JF, Wu XQ, Shen SY, Cui WY, Zhu YW (2018) Enhanced adsorption of phthalic acid esters (PAEs) from aqueous solution by alkylbenzene-functionalized polypropylene nonwoven and its adsorption mechanism insight. Chem Eng J 311:406–415

Zuo HG, Lin YS, Ma XX, Feng YH, Luo QH (2019) Preparation of a novel restricted access material combined to core-shell magnetic molecularly imprinted polymers for determination of dimethyl phthalate in soils. Soil Sediment Contam 28:529–546